Supporting information

Temperature-induced Absolute Energy Shift of the Electronic Spectrum in HgTe Nanocrystals

Tommaso Gemo[1,2$], Dario Mastrippolito[1,3$], Mariarosa Cavallo[1], Giorgia Strobbia[1], Albin Colle[1], Marco Paye[1], Jiho Roh[1], Adrien Khalili[1], Clement Gureghian[1], Erwan Bossavit[1,3], Sandrine Ithurria[4], Yoann Prado[1], Sébastien Sauvage[5], Mathieu G. Silly[3], Nicolas Péré-Laperne[2], Debora Pierucci[1], Emmanuel Lhuillier[1*]

[1] Sorbonne Université, CNRS, Institut des NanoSciences de Paris, 4 place Jussieu, 75005 Paris, France.
[2] LYNRED, Actipole - CS 10021, 364 route de Valence, 38113 Veurey-Voroize, France
[3]Synchrotron SOLEIL, L'Orme des Merisiers, Départementale 128, 91190 Saint-Aubin, France.
[4] Laboratoire de Physique et d'Etude des Matériaux, ESPCI, PSL Research University, Sorbonne Université, CNRS, 10 rue Vauquelin, 75005 Paris, France.
[5]Centre de Nanosciences et de Nanotechnologies, CNRS, Université Paris-Saclay, C2N, Palaiseau 2110, France.

$ these two authors have equal contributions

*To whom correspondence should be sent: el@insp.upmc.fr

Table of contents

1. Methods

Chemicals: Mercury chloride ($HgCl_2$, Alfa Aesar), tellurium powder (Te, Alfa Aesar, 99.99%), trioctylphosphine (TOP, thermofisher scientific, 90%), oleylamine (OLA, Acros, 80-90%), octadecene (ODE, Acros Organics, 90%), dodecanethiol (DDT, Sigma-Aldrich, 98%), methanol (MeOH, Carlo Erba, 99.8%), acetone (VWR), absolute ethanol (EtOH, VWR), isopropanol (IPA, VWR), toluene (Carlo Erba, 99.3%), N,N dimethylformamide (DMF, VWR), 2-mercaptoethanol (MPOH, Merck, >99%). All chemicals are used as received, except oleylamine, which is centrifuged before use. **Mercury compounds are highly toxic. Handle them with special care.**

1 M TOP:Te precursor: 6.35 g of Te powder was mixed in 50 mL of TOP in a three-neck flask. The flask was kept under vacuum at room temperature for 5 min, and then the temperature was raised to 100 °C. Furthermore, degassing of the flask was conducted for the next 20 min. The atmosphere was switched to Ar, and the temperature was raised to 275 °C. The solution was stirred until a clear orange coloration was obtained. The flask was cooled down to room temperature, and the color switched to yellow. Finally, this solution was transferred to a nitrogen-filled glove box for storage.

HgTe 6k: synthesis is inspired by Ref.[1]. In a 100 mL three neck flask, 540 mg of $HgCl_2$ (2 mmol) and 50 mL of oleylamine are degassed under vacuum at 110 °C for 1h. Then, the atmosphere is switched to N_2, and the temperature stabilizes at 58 °C. Meanwhile, 2 mL of TOP:Te (1 M) is extracted from the glove box and mixed with 8 mL of oleylamine. Then, the TOP:Te solution is quickly injected. After 3 min, 10 mL of a mixture of 10% DDT in toluene is injected, and a water bath is used to quickly decrease the temperature. The content of the flask is split over 4 centrifuge tubes. MeOH is added, and the solution is sonicated for 3 min. After centrifugation, the formed pellets are redispersed in one centrifuge tube with toluene. The solution is precipitated a second time with absolute EtOH and sonicated for 3 min. Again, the formed pellet is redispersed in toluene. Then, the NCs are centrifuged in pure toluene to get rid of the lamellar phase. The solid phase is discarded.

HgTe 4k: In a 100 mL three-neck flask, 540 mg of $HgCl_2$ (2 mmol) and 50 mL of oleylamine are degassed under vacuum at 110 °C for 1h. Then, the atmosphere is switched to N_2, and the temperature stabilizes at 82 °C. Meanwhile, 2 mL of TOP:Te (1 M) is extracted from the glove box and mixed with 8 mL of oleylamine. Then, the TOP:Te solution is quickly injected. After 3 min, 10 mL of a mixture of 10% DDT in toluene is injected, and a water bath is used to quickly decrease the temperature. The content of the flask is split over 4 centrifuge tubes. MeOH is added, and the solution is sonicated for 3 min. After centrifugation, the formed pellets are redispersed in one centrifuge tube with toluene. The solution is precipitated a second time with absolute EtOH and sonicated for 3 min. Again, the formed pellet is redispersed in toluene. Then, the NCs are centrifuged in pure toluene to get rid of the lamellar phase. The solid phase is discarded.

HgTe 3k: In a 100mL three-neck flask, 543 mg of $HgCl_2$ and 50 mL of oleylamine were degassed under vacuum at 110°C. Meanwhile, 2 mL of TOP:Te (1M) was extracted from the glove box and mixed with 8 mL of oleylamine. After the flask atmosphere was switched to N_2 and the temperature stabilized at 110°C, the TOPTe solution was quickly injected. After 3 mins, 10 mL of a mixture of DDT in toluene (10% of DDT) was injected, and a water bath was used to quickly decrease the temperature. The content of the flask was split over 3 centrifuge tubes, and MeOH was added. After centrifugation, the formed pellet was redispersed in one centrifuge tube with chloroform. The solution was precipitated a second time using ethanol. The formed pellet was redispersed in

chlorobenzene. At this step, the nanocrystals were centrifuged in pure toluene to get rid of the lamellar phase. The solid phase was discarded. The solution is filtered with a 0.2 µm filter.

NC ink preparation: Before deposition, the NCs are prepared into a concentrated ink. A volume of 0.65/OD of the prepared HgTe solution, 0.2 mL of DMF, and 0.8 mL of exchange solution (30 mg $HgCl_2$ and 2 mL of MPOH in 18 mL of DMF) were added to a centrifuge tube and agitated thoroughly with vortex mixing and sonication. 5 mL of hexane was added to wash the solution, agitated thoroughly without sonication, and then discarded after phase separation. The QDs were then precipitated by adding 4 mL of toluene and centrifuging at 6000 rpm for 3 min. The remaining pellet was dried for 60 s under vacuum, then redispersed in 250 µL of DMF by agitating and sonicating.

NC film preparation: The NCs are then deposited on a gold-coated silicon substrate. A few drops of filtered DMF were deposited on the substrate and left for 30 s, then dried by spin coating at 4000 rpm for 30 s. Then, 15 µL of previously prepared ink was deposited on the substrate and spin-coated at 1250 rpm for 180 s, then 6000 rpm for 60 s.

X-ray photoemission spectroscopy (XPS): Photoemission spectroscopy measurements were performed using a PHI GENESIS setup. The samples were introduced into the load-lock chamber and degassed until a vacuum of $2 \cdot 10^{-7}$ mbar was reached. They were then transferred to the analysis chamber (base pressure $2 \cdot 10^{-9}$ mbar). The spectra were recorded using a monochromatic Al Kα X-ray source (hv=1486.6 eV) with a spot size of 100 µm in a normal emission configuration at room temperature. No charge compensation was applied. Core-level spectra (Hg 4f, Te 3d, and Te 4d) were acquired with a pass energy of 27 eV. The zero-binding energy (BE) reference, corresponding to the Fermi level, was calibrated using the leading edge of a clean Ag foil.

Synchotron-based XPS: For synchrotron-based XPS, the TEMPO beamline of synchrotron SOLEIL was used.[2] Samples were introduced in the preparation chamber and degassed until a vacuum below 10^{-9} mbar was reached. Then, samples were introduced into the analysis chamber. The signal was acquired by a MBS A-1 photoelectron analyzer, with acquisitions performed with a pass energy of 50 eV within the detector. Photon energies of 700 eV and 150 eV were used. The zero BE reference was taken at the leading edge of a clean Au film.

XPS analysis: XPS spectra were decomposed using pseudo-Voigt functions (20% weighted Lorentzian contribution) using the CASAXPS software package. A linear background was used for Hg 4f and Te 4d, while a Tougaard background was used for Te 3d.

To evaluate the shift of core levels spectra at low temperature relative to room temperature, the peaks are overlapped by aligning both the low-binding energy background and the peak positions. This ensures a consistent determination of the spectra shift across temperatures.

To fit the valence band data, we first subtract the background (typically the signal value near the Fermi energy) and normalize the signal. We then systematically perform a linear fit of the valence edge between 15 and 85% of the normalized magnitude.[3] The intercept of this line with the background is taken as the valence band position relative to the Fermi level ($V_b - E_F$). To estimate the error of this procedure, we use a second method in which the low-temperature data are shifted along the x-axis to overlap the room-temperature data. From this comparison, we estimate the uncertainty to be approximately 15 meV.

2. 14-band k.p modeling of the electronic structure.

The 14-band **k.p** model (referred to as kp14 in what follows) used to describe the electronic structure is detailed in Ref.[4]. The same single parameter set is used for all energies and temperatures. The consideration of 14 bands provides a more realistic description of the dispersion relation from the zone center to around 15% of the Brillouin zone, as compared to a simple effective mass parabolic dispersion approach.

Figure S 1 illustrates the strong non-parabolicities by comparing parabolic and a 14-band k.p $E_{LH}(k)$ dispersions. A parabolic dispersion is taken as $E(k) = \frac{\hbar^2}{2m^*}k^2$ where m^* is the considered effective mass and $\hbar$ the reduced Plank constant. **Figure S 1**a shows that the very small effective mass at 293 K of $m^* = 0.0057m_0$, originating from the red-shift bandgap at this temperature, cannot describe the more realistic kp14 dispersion beyond around 1% only of the reciprocal space. The effective mass of $m^* = 0.0134m_0$ at 0 K, nearly twice as much as the one at 293 K, due to the blue-shift of the HH-Γ_6 energy difference, is also considered and shows an even worse discrepancy with kp14 model. Considering an effective mass of $m^* = 0.03m_0$ as considered in **Figure S 1**b is no longer suited to describe the quasi-linear dispersion relation over the investigated energy range. Quantitatively, the ratio between the parabolic and kp14 dispersions in this case is reported in **Figure S 1**c, showing a strong deviation away from 0.6 eV energy.

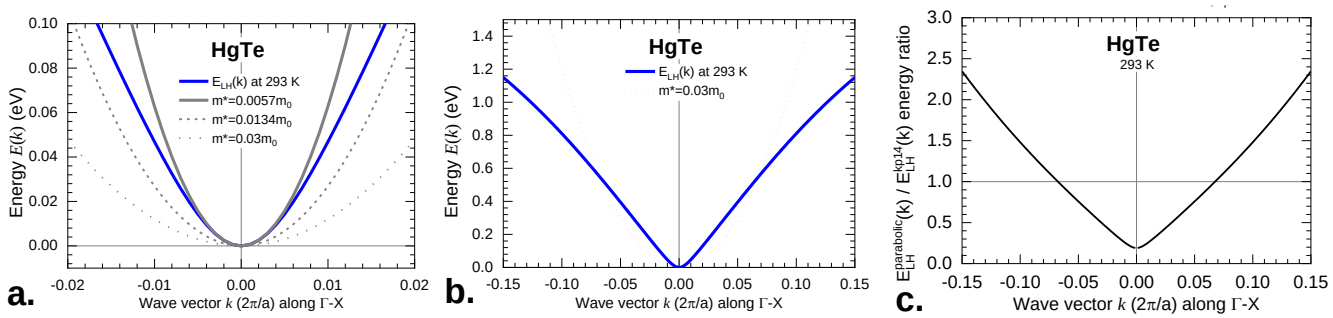

Figure S 1 Comparison between parabolic and 14-band k.p $E_{LH}(k)$ dispersions. *a. Dispersion $E_{LH}(k)$ close to the Brillouin zone center in the 14-band k.p model (blue full line) as compared to a single effective mass parabolic dispersion with room temperature $0.0057\,m_0$ (full gray line), low temperature $0.013m_0$ (gray dashed line), and heavier $0.03m_0$ (gray dotted line) effective masses. b. Comparison between a parabolic dispersion with $0.03m_0$ effective mass and $E_{LH}(k)$ of the kp14 model away from the Brillouin zone center at larger energies then a.c. Ratio of the two energies plotted in b. quantifying the discrepancy between the two parabolic and kp14 dispersions.*

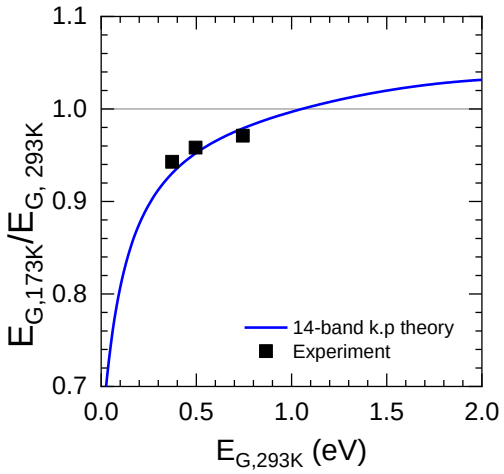

***Figure S 2 Measured and theoretical band gap shifts with lowering temperature**. Comparison between the band gap relative red-shifts with temperature from Fig. 4 (full squares) and the band gap shifts as calculated in the 14-band k.p model (full blue line). A value of 1, lower than 1, or larger than 1 indicates no shift with respect to the 293 K reference temperature, a redshift, and a blue shift, respectively.*

Figure S 2 illustrates the adequacy of the 14-band k.p model when confronted with the red-shifts observed experimentally in Figure 4, when the temperature is lowered from 293 K to 173 K. The experimental band gaps of three nanocrystal sizes are reported as full squares. The calculated $E_G(T) = E_{LH}(T) - E_{HH}(T)$ band gap at temperature T is reported as a full blue line as a function of $E_G(293K)$.

3. Temperature dependence of the current

To track the temperature dependence of the current, a film of NC has been deposited onto interdigitated electrodes (25 pairs, spaced by 10 µm, and 2.5 mm long). The sample is mounted onto the cold finger of a cryostat. A constant bias is applied, and the current is recorded thanks to a Keithley 2634 sourcemeter. Care is taken that sample resistance is not limited by contact.

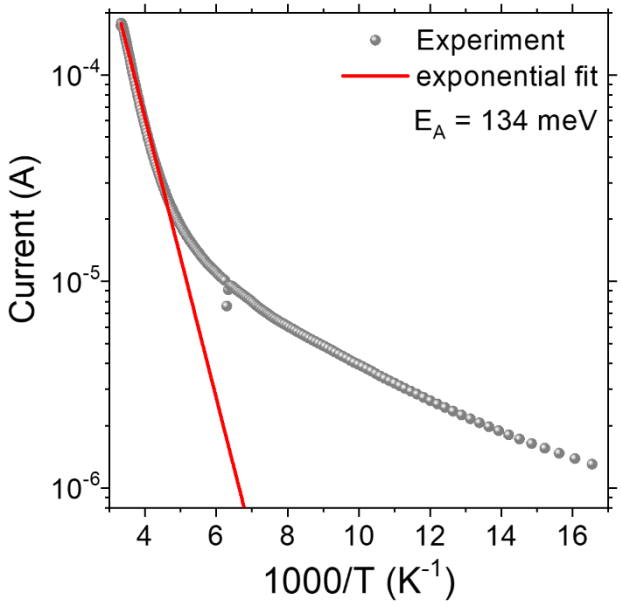

Figure S 3 Current as a function of temperature for HgTe 4k NC film.

4. Thermal shift of the absolute energy electronic structure.

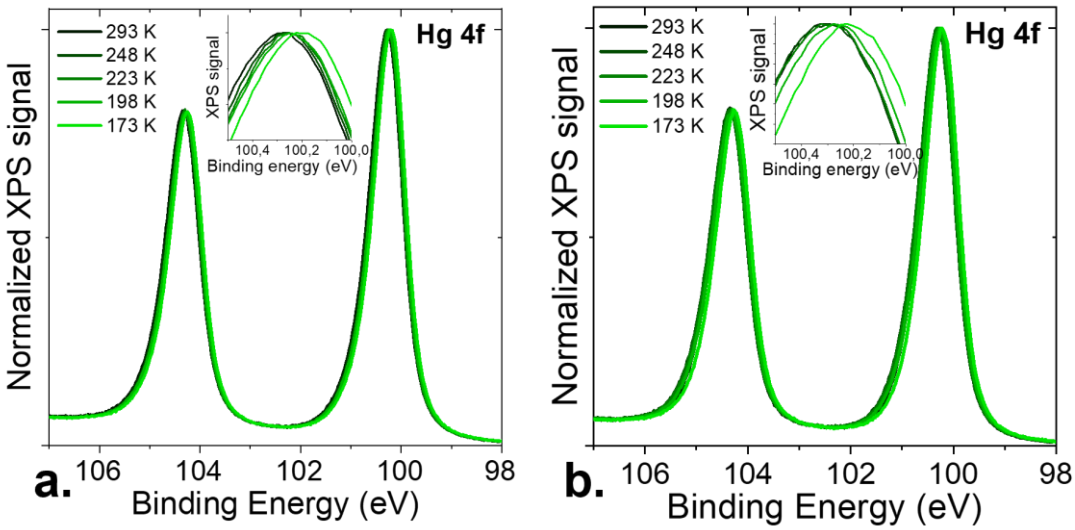

Figure S 4 Thermal Shift for HgTe 3k and 6k*. a. (resp b.) Hg 4f core level acquired at 1486.6 eV for HgTe 3k (resp 6k) NCs under various temperatures. Inset in both figures is a zoom on the Hg* $4f_{7/2}$ *peak to better highlight its shift with temperature.*

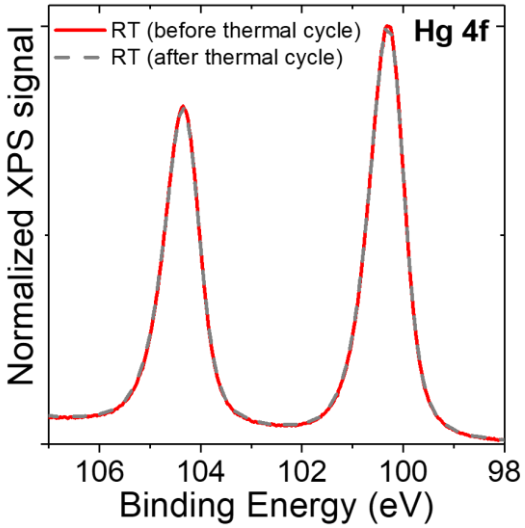

Figure S 5 Reversibility of the shift*. Hg 4f core level from HgTe 6k NCs at room temperature, before and after a cooling cycle.*

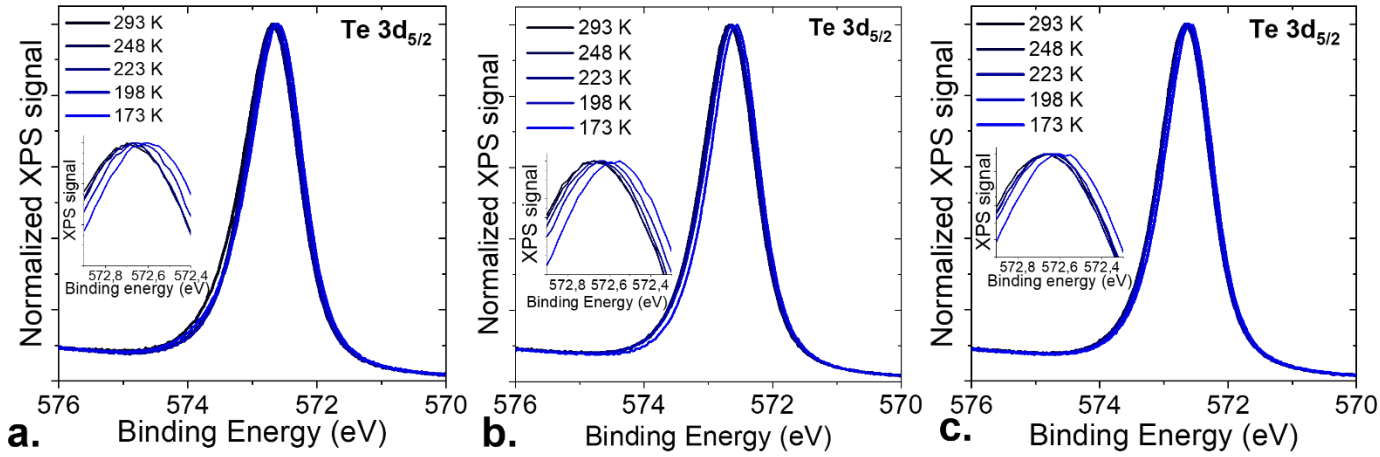

Figure S 6 Shift of the Te 3d core level as a function of temperature*. Te 3d core level acquired at 1486.6 eV for HgTe 6k (a), HgTe 4k (b.), HgTe 3k (c.) NCs under various temperatures. Inset in both figures is a zoom on the Te 3d$_{5/2}$ peak to better highlight its shift with temperature.*

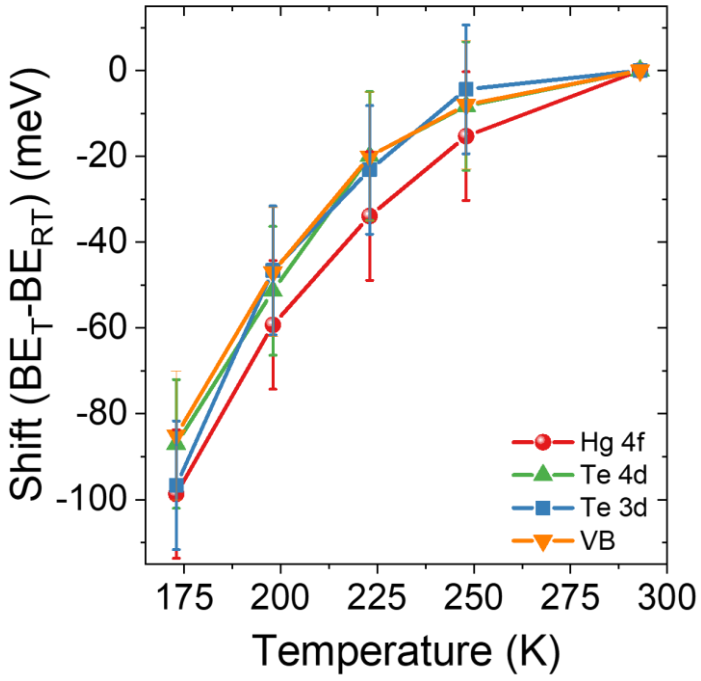

Figure S 7 Rigid shift of the spectra with temperature. *Shifts of the Hg 4f, Te 3d, and Te 4d core levels, and the valence band with temperature for HgTe 4k NCs.*

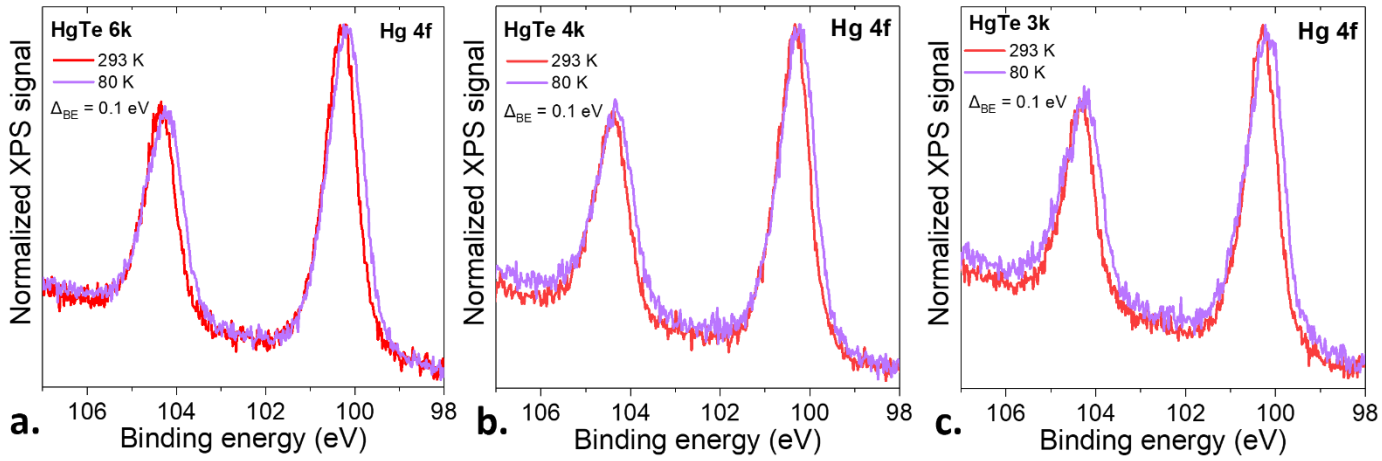

Figure S 8 Confirmation of the effect on synchrotron setup. *Hg 4f core level acquired at 150 eV for HgTe 6k (a), HgTe 4k (b.), HgTe 3k (c.) NCs acquired at room temperature and 80 K.*

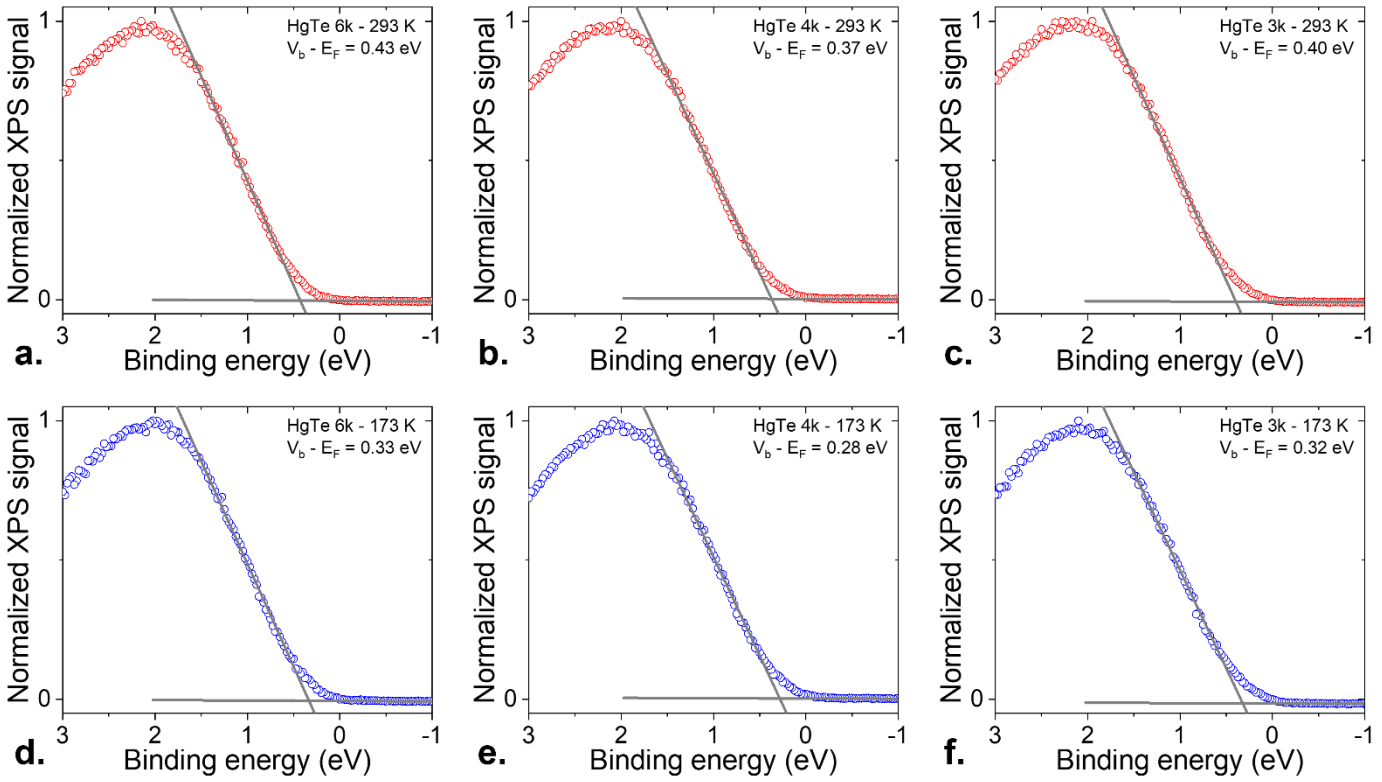

Figure S 9 Valence band signal*. Photoemission signal relative to the valence band from HgTe 6k (a, resp. d), HgTe 4k (b, resp. e), HgTe 3k (c, resp. f). Data have been measured at room temperature (resp. 173 K).*

5. References

(1) Keuleyan, S.; Lhuillier, E.; Guyot-Sionnest, P. Synthesis of Colloidal HgTe Quantum Dots for Narrow Mid-IR Emission and Detection. *J. Am. Chem. Soc.* **2011**, *133* (41), 16422–16424. https://doi.org/10.1021/ja2079509.

(2) Polack, F.; Silly, M.; Chauvet, C.; Lagarde, B.; Bergeard, N.; Izquierdo, M.; Chubar, O.; Krizmancic, D.; Ribbens, M.; Duval, J. -P.; Basset, C.; Kubsky, S.; Sirotti, F. TEMPO: A New Insertion Device Beamline at SOLEIL for Time Resolved Photoelectron Spectroscopy Experiments on Solids and Interfaces. *AIP Conf. Proc.* **2010**, *1234* (1), 185–188. https://doi.org/10.1063/1.3463169.

(3) Lazzari, R. *I4P*: An *Igor Pro* Suite for Photoemission Analysis. *J. Electron Spectrosc. Relat. Phenom.* **2024**, *275*, 147474. https://doi.org/10.1016/j.elspec.2024.147474.

(4) Moghaddam, N.; Gréboval, C.; Qu, J.; Chu, A.; Rastogi, P.; Livache, C.; Khalili, A.; Xu, X. Z.; Baptiste, B.; Klotz, S.; Fishman, G.; Capitani, F.; Ithurria, S.; Sauvage, S.; Lhuillier, E. The Strong Confinement Regime in HgTe Two-Dimensional Nanoplatelets. *J. Phys. Chem. C* **2020**, *124* (42), 23460–23468. https://doi.org/10.1021/acs.jpcc.0c07533.